inorganics

MDPI

Article

2,1,3-Benzoselenadiazole as Mono- and Bidentate N-Donor for Heteroleptic Cu(I) Complexes: Synthesis, Characterization and Photophysical Properties

Valentina Ferraro [1], Fabian Hoffmann [2], Olaf Fuhr [3], Burkhard Luy [2,*] and Stefan Bräse [1,4,*]

[1] Institute of Organic Chemistry (IOC), Karlsruhe Institute of Technology (KIT), Kaiserstrasse 12, 76131 Karlsruhe, Germany; valentina.ferraro@kit.edu
[2] Institute for Biological Interfaces 4 (IBG-4), Karlsruhe Institute of Technology (KIT), Kaiserstrasse 12, 76131 Karlsruhe, Germany; fabian.hoffmann@kit.edu
[3] Institute of Nanotechnology (INT) and Karlsruhe Nano Micro Facility (KNMFi), Karlsruhe Institute of Technology (KIT), Kaiserstrasse 12, 76131 Karlsruhe, Germany; olaf.fuhr@kit.edu
[4] Institute of Biological and Chemical Systems—Functional Molecular Systems (IBCS-FMS), Karlsruhe Institute of Technology (KIT), Kaiserstrasse 12, 76131 Karlsruhe, Germany
* Correspondence: burkhard.luy@kit.edu (B.L.); braese@kit.edu (S.B.)

Abstract: Mono- and binuclear Cu(I) complexes were isolated employing 2,1,3-benzoselenadiazole (BSeD) as the N-donor ligand, and triphenylphosphine or bis[(2-diphenylphosphino)phenyl] ether (DPEphos) as P-donors. Then, ^{77}Se NMR was measured for the free ligand and the corresponding Cu(I) derivatives, and the related signal was downshifted by 12.86 ppm in the case of [Cu(BSeD)$(PPh_3)_2(ClO_4)$], and around 15 ppm for the binuclear species. The structure of [Cu(BSeD)$(PPh_3)_2(ClO_4)$] and [$Cu_2(\mu_2$-BSeD)$(DPEphos)_2(ClO_4)_2$] was confirmed by single-crystal X-ray diffraction. The geometry of the Cu(I) complexes was optimized through DFT calculations, and the nature of the Cu···O interaction was investigated through AIM analysis. The three Cu(I) complexes were characterized by intense absorption under 400 nm and, after being excited with blue irradiation, [Cu(BSeD)$(PPh_3)_2(ClO_4)$] and [$Cu_2(\mu_2$-BSeD)$(PPh_3)_4(ClO_4)_2$] exhibited weak red emissions centered at 700 nm. The lifetimes comprised between 121 and 159 µs support the involvement of triplet excited states in the emission process. The photoluminescent properties of [Cu(BSeD)$(PPh_3)_2(ClO_4)$] were supported by TDDFT computations, and the emission was predicted at 710 nm and ascribed to a metal-to-ligand charge transfer (^{3}MLCT) process, in agreement with the experimental data.

Keywords: Cu(I) complexes; 2,1,3-benzoselenadiazole; phosphines; ^{77}Se NMR; DFT calculations

Citation: Ferraro, V.; Hoffmann, F.; Fuhr, O.; Luy, B.; Bräse, S. 2,1,3-Benzoselenadiazole as Mono- and Bidentate N-Donor for Heteroleptic Cu(I) Complexes: Synthesis, Characterization and Photophysical Properties. *Inorganics* **2024**, *12*, 201. https://doi.org/10.3390/inorganics12080201

Academic Editor: Santo Di Bella

Received: 31 May 2024
Revised: 21 July 2024
Accepted: 23 July 2024
Published: 25 July 2024

1. Introduction

Benzochalcogendiazoles, such as 2,1,3-benzothiadiazole (BTD) and 2,1,3-benzoselenadiazole (BSeD), are currently being widely investigated for optoelectronic applications, such as organic light-emitting diodes (OLEDs) and photovoltaics [1–4], as well as for bioimaging [5–7]. Their well-ordered structures, obtained due to both chalcogen and π-π stacking interactions, together with the strong withdrawing ability of these π-extended heteroarenes enable their use as building blocks in organic donor–acceptor (D-A) dyes [8–11]. In addition, the presence of two nitrogen atoms in their skeleton makes them suitable candidates to be used as ligands for a wide variety of metal centers. For instance, bis-triazolyl benzochalcogendiazoles exhibit good sensing performance towards Cu(II), Ni(II), and Ag(I) due to their binding ability and the derived changes in their photoluminescent properties [12].

With all of this in mind, we previously studied the coordination of Cu(I) towards BTD, obtaining derivatives characterized by improved photophysical properties in terms of photoluminescent lifetimes τ and quantum yields (PLQYs) [13]. Following these results and our interest in using Cu(I) as an emitter [14,15], we deemed it interesting to study the effect of a heavier chalcogen atom, i.e., selenium, in the skeleton of the N-donor ligand and

the related heteroleptic Cu(I) complexes. Compared to BTD, with regard to which some reports together with the photophysical properties of corresponding derivatives [16,17] are present in the literature, the use of BSeD as an N-donor ligand is quite rare and, to the best of our knowledge, no example of coordination towards Cu(I) has ever been described. The few examples reported in the literature focus on W(0), Re(0), Ru(II), Os(II), Ir(III), Ag(I), and Hg(II) as metal centers [18–24].

Herein, we report the synthesis of three mono- and binuclear heteroleptic Cu(I) complexes using BSeD as the N-donor and phosphines such as PPh_3 and bis[(2-diphenylphosphino) phenyl] ether (DPEphos) as P-donors. The Cu(I) derivatives were characterized by common spectroscopic techniques, including ^{77}Se NMR, and weak red emissions due to metal-to-ligand charge transfer (^{3}MLCT) mechanisms were detected for the Cu(I) species with PPh_3 in the coordination sphere.

2. Results and Discussion

The synthesis of 2,1,3-benzoselenadiazole (BSeD) was completed by condensation of *o*-phenylenediamine and SeO_2, following a reported procedure [7]. In accordance with the results previously reported using 2,1,3-benzothiadiazole as the N-donor ligand [13], the mononuclear complex $[Cu(BSeD)(PPh_3)_2(ClO_4)]$ was synthesized starting from CuCl, PPh_3, and BSeD, in the presence of $AgClO_4$ (see Scheme 1). Binuclear complexes with the general formulae $[Cu_2(\mu_2\text{-BSeD})(PPh_3)_4(ClO_4)_2]$ and $[Cu_2(\mu_2\text{-BSeD})(DPEphos)_2(ClO_4)_2]$ were synthesized according to the same synthetic procedure, except for the reduction of the equivalents of ligand to 0.5. The presence of both N- and P-donor ligands was confirmed by ^{1}H, ^{13}C, and ^{31}P{^{1}H} NMR spectra. Broadened signals due to fluxional behavior in solution were observed. This was particularly evident in the case of the ^{31}P signals. The proposed formula was supported by mass and IR spectra, as well as elemental analyses. In particular, the IR spectra supported the presence of the perchlorate owing to the intense stretchings $\nu_{Cl\text{-}O}$ observable between 1115 and 1090 cm^{-1}.

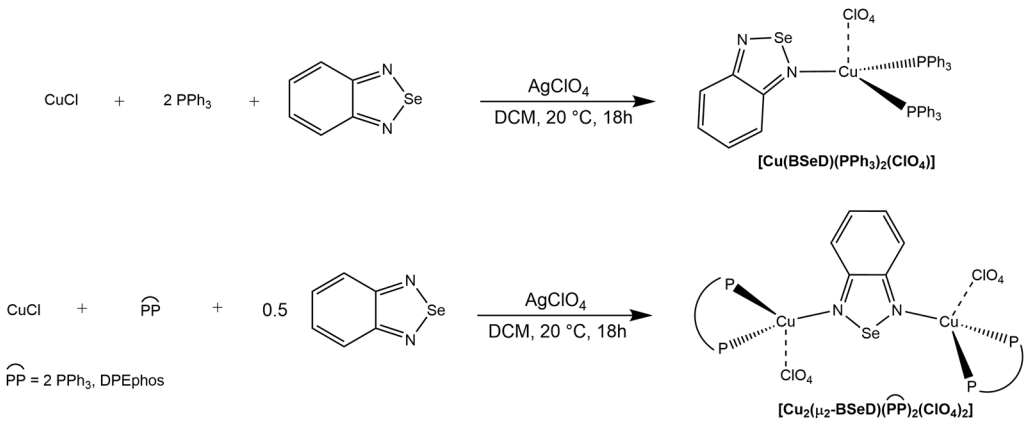

Scheme 1. Synthesis of mono- and binuclear Cu(I) complexes.

To further confirm the presence of BSeD, ^{77}Se NMR was collected for both the ligand and the three Cu(I) complexes. As observable in Figure 1, the signal of the free BSeD was localized at 1511.26 ppm, and it was downshifted by 12.86, 14.89, and 15.47 ppm due to the coordination to the metal center. In particular, the difference between the two signals was lower for the mononuclear $[Cu(BSeD)(PPh_3)_2(ClO_4)]$ compared to the binuclear $[Cu_2(\mu_2\text{-BSeD})(PPh_3)_4(ClO_4)_2]$ and $[Cu_2(\mu_2\text{-BSeD})(DPEphos)_2(ClO_4)_2]$. Furthermore, ^{77}Se chemical shifts similar to the former were observed for analog Ru(II) complexes using BSeD as the monodentate ligand [23].

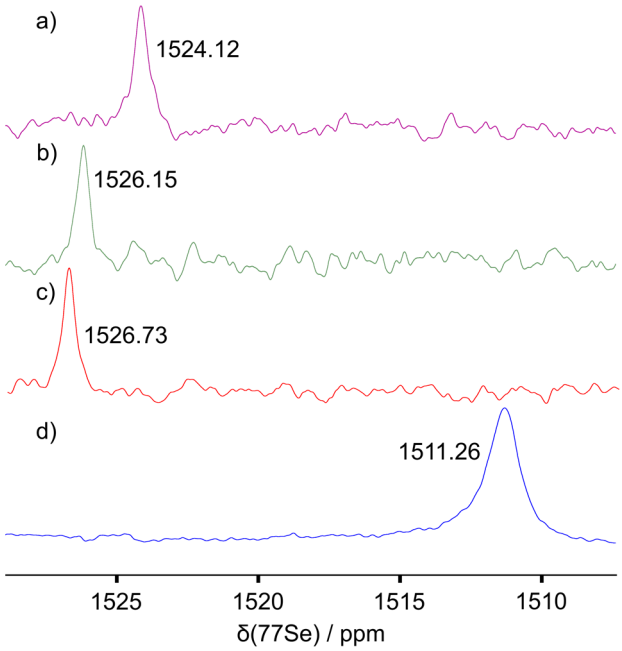

Figure 1. The 1D ^{77}Se spectra of (**a**) [Cu(BSeD)$(PPh_3)_2(ClO_4)$], (**b**) [$Cu_2(\mu_2$-BSeD$)(PPh_3)_4(ClO_4)_2$], (**c**) [$Cu_2(\mu_2$-BSeD$)$(DPEphos$)_2(ClO_4)_2$], and (**d**) the ligand BSeD. Peak annotations give chemical shift values in ppm defined relative to the deuterium resonance of $CDCl_3$ as the reference and using the internal Bruker spectrometer referencing.

Crystals of [Cu(BSeD)$(PPh_3)_2(ClO_4)$] and [$Cu_2(\mu_2$-BSeD$)$(DPEphos$)_2(ClO_4)_2$] suitable for X-ray diffraction were collected from the slow diffusion of dichloromethane/diethyl ether solutions. The molecular structure of the complexes and the crystal data and structural refinement are, respectively, presented in Figure 2 and Table 1. Selected bond lengths and angles are collected in Tables S1 and S2. Both Cu(I) complexes crystallized in the monoclinic system (C*c* and C2/*c* space groups), and the metal center was four-coordinated to two phosphorus and one nitrogen atoms in a distorted tetrahedral geometry. Despite the soft Pearson character of Cu(I) and the selenium atom, BSeD always acts as an N-donor ligand [13,18–24]. The remaining coordination site was balanced by the perchlorate anion, which was incorporated through long interactions, as in the previously reported derivatives with BTD [13]. The structure of [Cu(BSeD)$(PPh_3)_2(ClO_4)$] was non-centrosymmetric, and the Flack parameter was refined to −0.007 (7) [25].

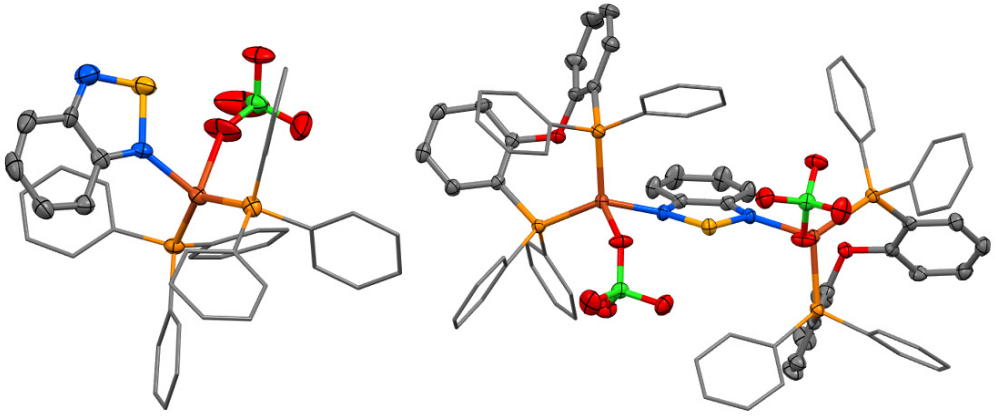

Figure 2. Molecular structures of [Cu(BSeD)$(PPh_3)_2(ClO_4)$] and [$Cu_2(\mu_2$-BSeD$)$(DPEphos$)_2(ClO_4)_2$]. Hydrogen atoms are omitted for clarity. Color map: Cu, orange; C, grey; N, blue; O, red; P, light orange; Cl, green; Se, yellow. Ellipsoids are drawn at 50% probability level.

Table 1. Crystal data and structure refinement [Cu(BSeD)$(PPh_3)_2(ClO_4)$] and [$Cu_2(\mu_2$-BSeD) $(DPEphos)_2(ClO_4)_2$].

Empirical Formula	**$C_{42}H_{34}ClCuN_2O_4P_2Se$**	**$C_{78}H_{60}Cu_2N_2O_{10}P_4SeC_{l2}$**
Formula weight	870.60	1586.10
Temperature/K	180	
Crystal system	Monoclinic	
Space group	*Cc*	*C*2/*c*
a/Å	12.5156 (8)	15.8430 (5)
b/Å	19.0888 (15)	18.1763 (5)
c/Å	16.3818 (10)	24.8971 (9)
β/°	95.746 (5)	99.158 (3)
Volume/$Å^3$	3894.1 (5)	7078.2 (4)
Z	4	4
ρ_{calc} g/cm^3	1.485	1.488
μ/mm^{-1}	1.691	1.343
F(000)	1768.0	3232.0
Crystal size/mm^3	0.18 × 0.04 × 0.03	0.28 × 0.2 × 0.16
Radiation	MoKα (λ = 0.71073)	
2Θ range for data collection/°	3.906 to 58.554	3.314 to 69.314
Index ranges	$-16 \leq h \leq 16$, $-25 \leq k \leq 24$, $-21 \leq l \leq 21$	$-16 \leq h \leq 24$, $-27 \leq k \leq 28$, $-38 \leq l \leq 39$
Reflections collected	23,862	44,786
Independent reflections	8024 [R_{int} = 0.0468, R_{sigma} = 0.1472]	14,221 [R_{int} = 0.0462, R_{sigma} = 0.1071]
Indep. reflections with $I \geq 2\sigma$ (I)	4400	7406
Data/restraints/parameters	8024/2/478	14221/0/447
Goodness-of-fit on F^2	0.774	0.838
Final R indexes [$I \geq 2\sigma$ (I)]	R_1 = 0.0362, wR_2 = 0.0625	R_1 = 0.0349, wR_2 = 0.0630
Final R indexes [all data]	R_1 = 0.0876, wR_2 = 0.0678	R_1 = 0.0947, wR_2 = 0.0694
Largest diff. peak/hole/e $Å^{-3}$	0.40/−0.58	0.46/−0.47
Flack parameter	−0.007 (7)	–
CCDC number	2353339	2353340

In the binuclear Cu(I) complexes, the BSeD acted as a bridging ligand between two Cu(I) centers. To the best of our knowledge, this bridging motif is quite uncommon, and it has been reported only for Ag(I) and η^6-cymene Ru(II) complexes [21,23], while in the other structures described in the literature, BSeD has acted as a monodentate ligand [18–20,22,24].

The distance between Cu(I) and the oxygen atom of the perchlorate was equal to 2.316 (4) Å for [Cu(BSeD)$(PPh_3)_2(ClO_4)$] and 2.2753 (12) Å for [$Cu_2(\mu_2$-BSeD)$(DPEphos)_2(ClO_4)_2$]. These values were higher compared to the BTD Cu(I) analog complex [13], and bigger than the sum of covalent radii, equal to 1.32 (4) Å for Cu and 0.66 (2) Å for O [26]. The Cu-O distance was in the same range as that observed for the analog BTD Cu(I) complex and similar derivatives reported in the literature, comprising values between 2.25 and 2.33 Å [13,27–30]. The distances between Cl1 and the oxygen atoms were shorter for the mononuclear [Cu(BSeD)$(PPh_3)_2(ClO_4)$] compared to the binuclear [$Cu_2(\mu_2$-BSeD)$(DPEphos)_2$ $(ClO_4)_2$], being in the 1.38–1.43 Å and 1.42–1.47 Å ranges, respectively. As concerns the selenium atom in BSeD, Se1 was equidistant from the two nitrogen atoms in the binuclear derivative, while the distance between Se1 and N1 was slightly longer (1.814 (4) Å) than Se1 and N2 (1.763 (5) Å) due to the coordination to the metal center in the mononuclear [Cu(BSeD)$(PPh_3)_2(ClO_4)$].

The geometry around the metal center was distorted between a tetrahedron and a vacant trigonal bipyramid due to the presence of a plane involving the two phosphorus and nitrogen atoms. The oxygen of the perchlorate lay in one of the axial positions, whereas the other one was vacant. The most distorted angles from the ideal 120° were P1-Cu1-P2 for [Cu(BSeD)$(PPh_3)_2(ClO_4)$] and N1-Cu1-P1 for [$Cu_2(\mu_2$-BSeD)$(DPEphos)_2(ClO_4)_2$], which were equal to 130.41 (6)° and 115.402 (16)°, respectively. On the other hand, the most acute angle in both cases was seen in N1-Cu1-O1(O2), being equal to 81.31 (18)° for the

former and 87.48 (5)° for the latter. Similar values were measured for the mononuclear [Cu(BSeD)(PPh_3)$_2$(ClO_4)] [13].

Regarding non-covalent interactions, [Cu(BSeD)(PPh_3)$_2$(ClO_4)] exhibited π-π′ stacking between the benzene ring of the BSeD and one of the phenyl rings of PPh_3 belonging to an adjacent molecule at a distance of 4.067 (3) Å (sym. op. x − 0.5, 1.5 − y, z − 0.5). Conversely, long range intermolecular π-π′ stacking interactions between the phenyl moieties of DPEphos were observed for the binuclear Cu(I) derivative, with the minimum distance between the centroids being around 4.494 Å. In addition, in both the Cu(I) complexes, intermolecular C-H···π interactions were detected between neighboring phenyl rings of the phosphines located at about 3 Å. One of the oxygen atoms of the perchlorate anion formed two hydrogen bonds with two different neighboring molecules of [Cu(BSeD)(PPh_3)$_2$(ClO_4)] (see Table S3 and Figure 3), whereas [Cu_2(μ_2-BSeD)(DPEphos)$_2$(ClO_4)$_2$] established two intra- (sym. op. −x, y, 0.5 − z generates the other half of the molecule) and two intermolecular hydrogen bonds (see Table S4 and Figure 4).

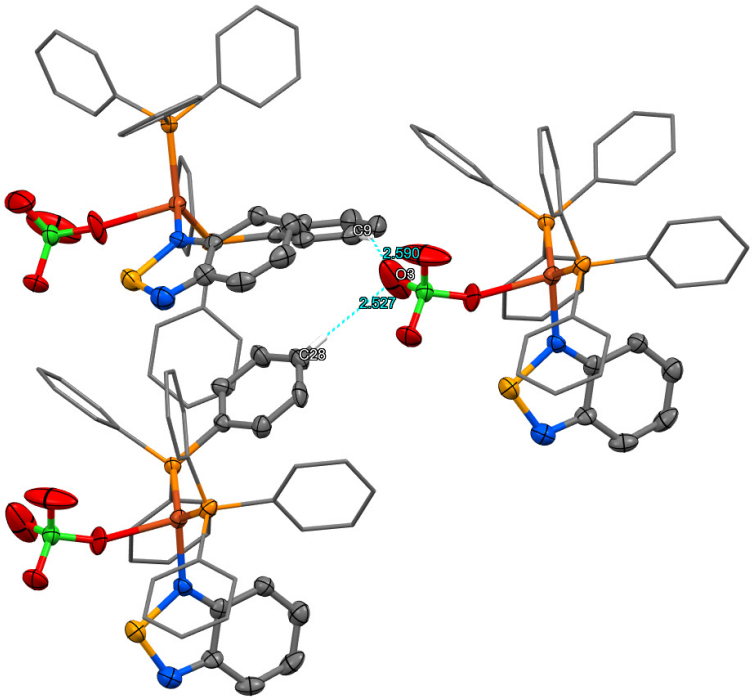

Figure 3. Intermolecular hydrogen bonding of [Cu(BSeD)(PPh_3)$_2$(ClO_4)].

As observable in Figure 5a, the selenium atom Se1 in [Cu(BSeD)(PPh_3)$_2$(ClO_4)] was involved in an intramolecular chalcogen bond with the O1 atom of the perchlorate anion, which could explain why the angles Cu1-O1-Cl1 (equal to 153.6 (4)°) and N1-Cu-O1 were so distorted from the ideal tetrahedral geometry. An intermolecular interaction between Se1 and one of the phenyl groups of PPh_3 was also observed. Similar considerations concerning the intramolecular interactions can be made for the binuclear Cu(I) derivative, where Se1 was involved in two chalcogen bonds with the O2 atoms of the perchlorate (see Figure 5b). However, Se1 was not involved in any intermolecular interactions in [Cu_2(μ_2-BSeD)(DPEphos)$_2$(ClO_4)$_2$].

The Cu(I) derivatives were intensely colored, both in powder and in concentrated dichloromethane solution (see Figure S1). The UV-vis spectra were characterized by absorptions below 350 nm, ascribable to the coordinated N- and P-donor ligands. As highlighted in Figure 6, the mononuclear [Cu(BSeD)(PPh_3)$_2$(ClO_4)] exhibited an absorption centered at 324 nm (ε = 14,400 mol^{-1} cm^{-1}), and this band was red-shifted for the binuclear derivatives, being centered at 334 nm (ε = 17,400–22,400 mol^{-1} cm^{-1}). This band can be ascribed to the ligand BSeD (λ_{abs} = 334 nm; ε = 16,430 mol^{-1} cm^{-1}), as can be observed from the inset in Figure 6. The absorption below 300 nm can be attributed to the $\pi^* \leftarrow \pi$ transitions of

the coordinated PPh_3 and DPEphos. Unfortunately, the metal-to-ligand charge transfer (MLCT) bands accounted for the intense color in the solid state and concentrated solutions could be detected only for $[Cu_2(\mu_2\text{-BSeD})(DPEphos)_2(ClO_4)_2]$ (see Figure S2 for the zoom of the region between 330 and 550 nm).

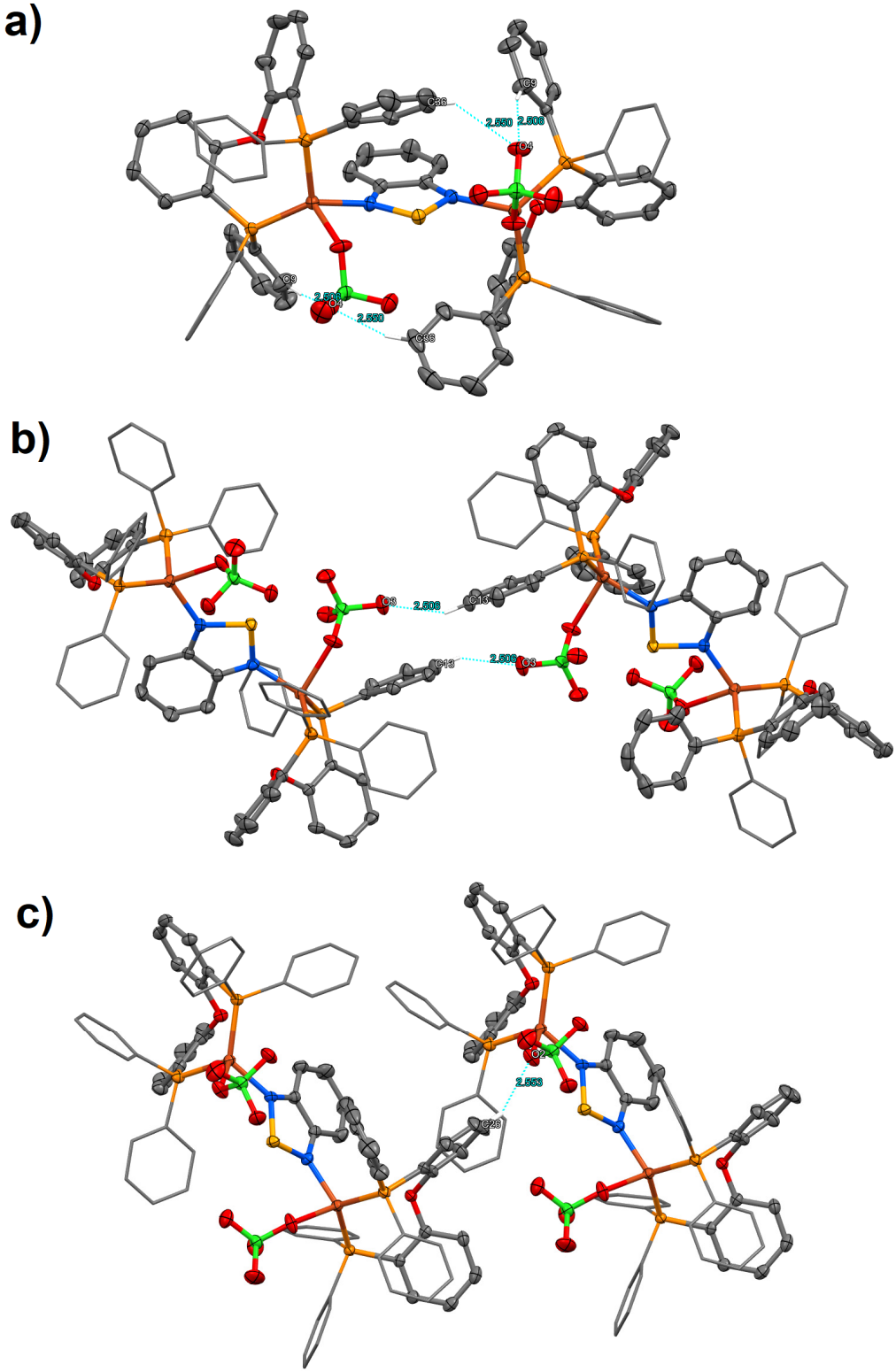

Figure 4. Intra- (**a**) and intermolecular (**b**,**c**) hydrogen bonds of $[Cu_2(\mu_2\text{-BSeD})(DPEphos)_2(ClO_4)_2]$.

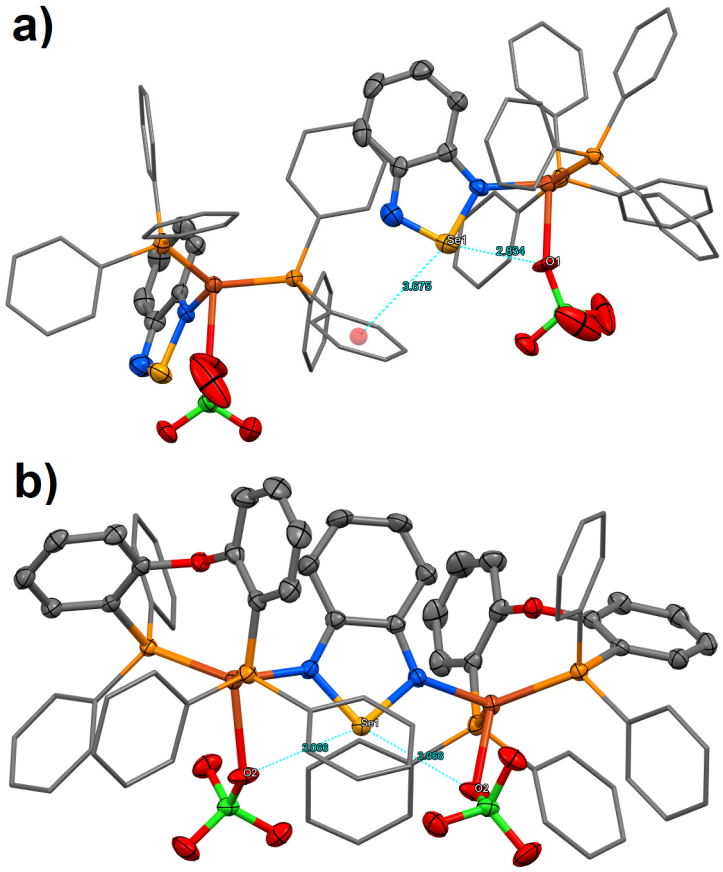

Figure 5. Intra- and intermolecular interactions of Se1 in (**a**) [Cu(BSeD)(PPh_3)$_2$(ClO_4)] and (**b**) [Cu_2(μ_2-BSeD)(DPEphos)$_2$(ClO_4)$_2$].

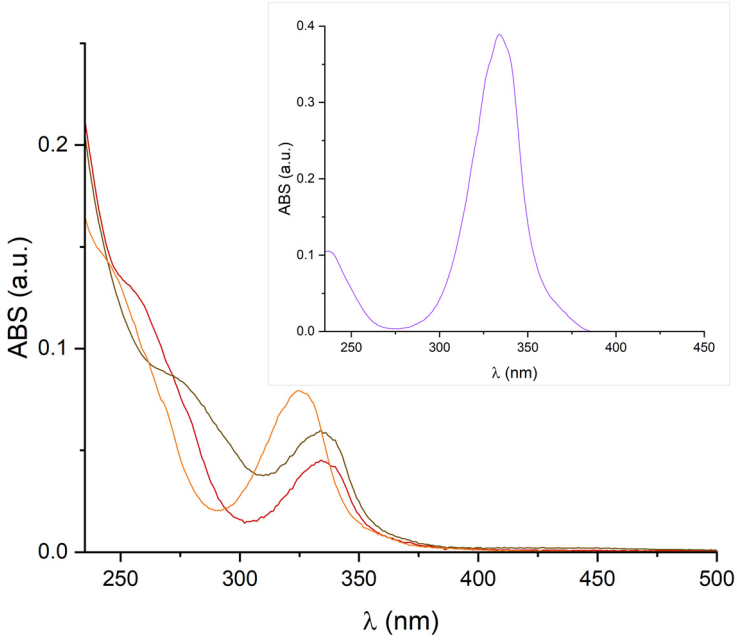

Figure 6. UV-vis spectra of [Cu(BSeD)(PPh_3)$_2$(ClO_4)] (orange line), [Cu_2(μ_2-BSeD)(PPh_3)$_4$(ClO_4)$_2$] (red line), and [Cu_2(μ_2-BSeD)(DPEphos)$_2$(ClO_4)$_2$] (yellow-brown line) collected in dichloromethane solutions at room temperature. Inset: UV-vis spectra of 2,1,3-benzoselenadiazole (BSeD, purple line) collected in dichloromethane solutions at room temperature.

The ground state structures of $[Cu(BSeD)(PPh_3)_2(ClO_4)]$ and $[Cu_2(\mu_2\text{-}BSeD)(DPEphos)_2(ClO_4)_2]$ were simulated using DFT calculations (TPPSh/def2-SVP), using dichloromethane as C-PCM and including the IR simulations to confirm the presence of a real minimum. The optimized structure obtained through DFT calculations was compared to the crystal structure, and the root-mean-square deviation (RMSD) was estimated to be 0.74 Å for the former and 0.57 Å for the latter. Selected bond lengths (Å) and angles (°) are collected in Tables S5 and S6 for comparison. The overlapping between the structures obtained via X-ray diffraction and DFT calculations is shown in Figures S3 and S4. Interestingly, the Cu-O distance was underestimated compared to the X-ray data for both the mono- and the binuclear Cu(I) complexes. Consequently, the Cl-O bond lengths of the perchlorate anion were overestimated in the calculation. The discrepancies between the experimental and the computed structures can be ascribed to the fact that the influence of the environment was neglected in the calculations, besides the latter being performed with dichloromethane as C-PCM. The interaction between Cu(I) and ClO_4^- in $[Cu(BSeD)(PPh_3)_2(ClO_4)]$ and $[Cu_2(\mu_2\text{-}BSeD)(DPEphos)_2(ClO_4)_2]$ was investigated through AIM analysis. As highlighted in Figures S5 and S6, a (3,1) critical bond was found between the metal center and one of the oxygen atoms of the perchlorate for both the Cu(I) complexes. The electron density (r), the energy density (E), and the Laplacian of the electron density ($\nabla^2 r$) were considered to obtain information regarding the nature of the interaction [31–33]. For both the Cu(I) derivatives, all these values were slightly positive (see Table S7 for the complete data), suggesting that the interaction Cu···O is ionic, as observed for the similar $[Cu(BTD)(PPh_3)_2(ClO_4)]$ [13].

The two Cu(I) complexes $[Cu(BSeD)(PPh_3)_2(ClO_4)]$ and $[Cu_2(\mu_2\text{-}BSeD)(PPh_3)_4(ClO_4)_2]$ with PPh_3 as the P-donor exhibited weak luminescent properties. The emission (PL) and excitation (PLE) spectra of $[Cu(BSeD)(PPh_3)_2(ClO_4)]$ and $[Cu_2(\mu_2\text{-}BSeD)(PPh_3)_4(ClO_4)_2]$ measured on a powder sample at room temperature are collected in Figure 7. Both the derivatives exhibited an emission in the red region centered at 700 nm, with an excitation that extended towards the visible range of the spectra in the blue region. Due to the low intensity of emission, no photoluminescent quantum yield (PLQY) could be measured. The photoluminescent lifetimes τ were 121 and 159 µs, respectively, for the mono- and the binuclear Cu(I) species. It is worth noting that for the mononuclear Cu(I) complex with BTD in the coordination sphere, lifetimes exceeding 1 ms were detected at room temperature [13]. The different photophysical behavior can be ascribed to the presence of a heavier chalcogen atom in the skeleton of the N-donor ligand, which increased the rate of the intersystem crossing and thus reduced the emissive lifetimes.

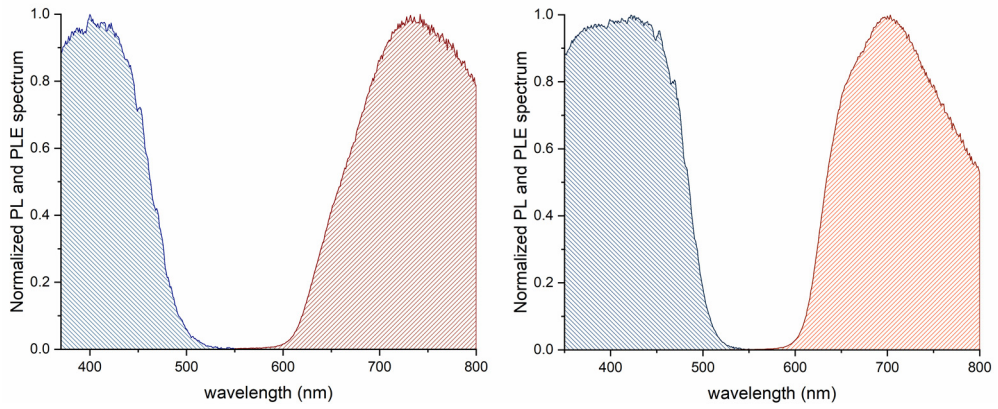

Figure 7. Normalized PL and PLE spectra of $[Cu(BSeD)(PPh_3)_2(ClO_4)]$ (**left**, λ_{ex} = 450 nm, λ_{em} = 700 nm) and $[Cu_2(\mu_2\text{-}BSeD)(PPh_3)_4(ClO_4)_2]$ (**right**, λ_{ex} = 450 nm, λ_{em} = 660 nm) collected in the solid state at room temperature.

The lifetimes in the hundreds of microseconds range suggest the involvement of triplet emitting states. Therefore, the emission of $[Cu(BSeD)(PPh_3)_2(ClO_4)]$ was investigated through TDDFT calculations at the same theoretical level, but introducing the spin-orbit

coupling effect. According to the computations, the emission was estimated at 710 nm, in agreement with the experimental data. The HOMO and LUMO plots are collected in Figure S7, supporting the metal-to-ligand charge transfer (^{3}MLCT) mechanism responsible for the emission. As observable for other Cu(I) complexes, the former was mostly localized on the metal center and the phosphines, with a small contribution of the heterocycle, whereas the latter was mostly localized on BSeD [34]. Since no emission was detected for $[Cu_2(\mu_2\text{-BSeD})(DPEphos)_2(ClO_4)_2]$, the photoluminescent properties were not computed for this complex.

3. Materials and Methods

The solvents were purchased from Fisher, if not stated otherwise. Dichloromethane was dried with the solvent purification system (SPS) from MBraun (model MB-SPS-800, Garching, Germany) and was degassed with argon before usage for 5 min. The precipitation of the Cu(I) complexes was performed with diethyl ether purchased from Merck (Darmstadt, Germany). The reagents *o*-phenylendiamine, CuCl and triphenylphosphine were purchased from Merck (Darmstadt, Germany). SeO_2 and DPEphos were obtained from Thermo Fisher Scientific (Waltham, MA, USA), while $AgClO_4$ was purchased from abcr (Karlsruhe, Germany). All chemicals were used without any further purification. The heteronuclear NMR spectra of the Cu(I) complexes were recorded in $CDCl_3$ purchased from Eurisotop (Saint-Aubin, France). All reactions were carried out using Schlenk techniques in an Ar atmosphere. Caution was taken with the perchlorate salts of transition metal complexes, as they are potentially explosive and should be handled with care.

General information concerning NMR, mass spectrometry, IR and elemental analyses, and melting points is detailed in the Supplementary Materials. Additional information on the experimental procedure is available via the Chemotion Repository [35].

Regarding the ^{77}Se NMR, 1D spectra with 32k data points and 1 scan were measured at 76.4497583 MHz on a Bruker (Ettlingen, Germany) Avance III 400 MHz spectrometer. The spectral range of ^{77}Se is approximately 3000 ppm. Therefore, we used a 1D with a specifically optimized saturation pulse for excitation (xyBEBOP with 500µs duration, an rf-amplitude of 10 kHz with a corresponding excitation bandwidth of 500 kHz) searching for the corresponding peaks within one measurement covering a sweep width of 5000 ppm [36]. Hereby, 128k data points and 128 scans were used. Spectra were processed using an exponential apodization function, adding a linewidth of 20 Hz to the signals.

3.1. Synthesis of 2,1,3-Benzoselenadiazole (BSeD)

The synthesis of 2,1,3-benzoselenadiazole (BSeD) was performed starting from *o*-phenylenediamine and SeO_2, according to a reported procedure [7]. A solution of *o*-phenylenediamine (1.08 g, 10 mmol) in 50 mL of ethanol was heated to reflux, and then a solution containing SeO_2 (1.17 g, 10.5 mmol) in 30 mL of hot water was added. The reaction mixture was refluxed for 2 h. Then, the solvent was removed under reduced pressure and the residue was dissolved in ethyl acetate and extracted with brine (3 × 50 mL). The organic phase was dried over Na_2SO_4, and the crude product was treated with pentane to afford a solid, which was filtered off, washed with 2 × 15 mL of pentane and dried in vacuo. Following this, 2,1,3-benzoselenadiazole (1.35 g, 7.40 mmol, 74% yield) was isolated as light brown solid.

m.p.: 76 °C. ^{1}H NMR (400 MHz, Chloroform-d [7.27 ppm], ppm) δ = 7.85–7.80 (m, 2H), 7.47–7.41 (m, 2H). ^{13}C NMR (100 MHz, Chloroform-d [77.0 ppm], ppm) δ = 160.5 (Cq, 2C), 129.4 (CH, 2C), 123.5 (CH, 2C). MS (EI, 70 eV, 20 °C), *m*/*z* (%): 186 (17), 185 (7), 184 (100) $[M + 1]^+$, 183 (5), 182 (47), 181 (17), 180 (18), 159 (5), 157 (30), 155 (14), 154 (5), 153 (6), 118 (5), 103 (5), 93 (8), 80 (11), 78 (5), 77 (14), 76 (12), 64 (6), 52 (10), 51 (10). HRMS (EI): *m*/*z* = calcd for $[C_6H_4N_2{}^{80}Se_1]^+$: 183.9534; found 183.9533. IR (ATR, $\tilde{\nu}$) = 3084 (vw), 3056 (vw), 3040 (vw), 3010 (vw), 1952 (w), 1930 (w), 1914 (w), 1824 (w), 1805 (w), 1745 (m), 1725 (m), 1706 (w), 1608 (w), 1501 (w), 1474 (w), 1439 (m), 1354 (m), 1348 (m), 1286 (w), 1220 (m), 1132 (w), 901 (s), 799 (vs), 739 (w), 706 (w), 594 (s), 556 (vs), 491 (vs) cm^{-1}.

Additional information on the experimental procedure is available via the repository Chemotion: https://dx.doi.org/10.14272/reaction/SA-FUHFF-UHFFFADPSC-AYTPIVIDHM-UHFFFADPSC-NUHFF-NUHFF-NUHFF-ZZZ (accessed on 22 July 2024).

Additional information on the characterization of the target compound is available via the repository Chemotion: https://dx.doi.org/10.14272/AYTPIVIDHMVGSX-UHFFFAOYSA-N.1 (accessed on 22 July 2024).

3.2. Synthesis of the Mononuclear Cu(I) Complex

Copper(I) chloride (50.0 mg, 505 µmol, 1.00 equiv) was dissolved in 10 mL of dry DCM together with triphenylphosphine (265 mg, 1.01 mmol, 2.00 equiv) under an Ar atmosphere. After stirring for 1 h, 2,1,3-benzoselenadiazole (92.5 mg, 505 µmol, 1.00 equiv) and silver(I) perchlorate (105 mg, 505 µmol, 1.00 equiv) were added, and the color of the solution rapidly changed to red. The mixture was stirred for 18 h at 20 °C and the precipitated AgCl was filtered off to afford a clear solution that was evaporated under reduced pressure. The obtained oil was treated with diethyl ether to afford a solid that was filtered off, washed with Et_2O (3 × 5 mL), and dried in vacuo. The product (357 mg, 390 µmol, 77% yield) was isolated as a dark orange powder.

m.p.: 160 °C (dec.) ^{1}H NMR (400 MHz, Chloroform-d [7.27 ppm], ppm) δ = 7.57 (dd, *J* = 3.2 Hz, *J* = 7.0 Hz, 2H, BSeD), 7.43–7.33 (m, 18H, PPh_3), 7.32–7.28 (m, 14H, BSeD + PPh_3). ^{31}P{^{1}H} NMR (162 MHz, ppm) δ = −0.83 (br. s). ^{13}C NMR (100 MHz, Chloroform-d [77.0 ppm], ppm) δ = 158.9 (Cq, 2C), 133.8 (d, *J* = 11 Hz, CH, 12C), 131.2 (d, *J* = 33 Hz, Cq, 6C), 130.6 (CH, 6C), 130.4 (CH, 2C), 129.1 (CH, 12C), 123.0 (CH, 2C). MS (FAB, 3-NBA), *m*/*z* (%): 689 (13), 688 (11), 687 (28), 686 (9) $[Cu(PPh_3)_2][ClO_4]^+$, 685 (22), 634 (6), 633 (15), 632 (6), 631 (15), 605 (5), 603 (10), 590 (20), 589 (54), 588 (43), 587 (100) $[Cu(PPh_3)_2]^+$, 425 (9) $[Cu(PPh_3)][ClO_4]$, 423 (8), 371 (9), 369 (11), 341 (6), 328 (5), 327 (30), 326 (13), 325 (63) $[Cu(PPh_3)]^+$, 263 (12), 262 (27) $[PPh_3]$, 185 (11), 183 (23) [BSeD], 154 (10) [3-NBA], 137 (5), 136 (8) [3-NBA]. IR (ATR, $\tilde{\nu}$) = 3070 (vw), 3055 (vw), 1514 (w), 1479 (w), 1435 (m), 1181 (w), 1160 (w), 1150 (w), 1115 (s), 1094 (vs), 1074 (w), 1035 (s), 997 (w), 973 (w), 922 (w), 904 (w), 744 (vs), 725 (w), 694 (vs), 618 (m), 601 (w), 517 (vs), 507 (vs), 490 (s), 428 (w), 391 (w) cm^{-1}. EA ($C_{42}H_{34}ClCuN_2O_4P_2Se$): Calcd C, 57.94; H, 3.94; N, 3.22. Found C, 56.53; H, 1.41; N, 2.83.

Additional information on the experimental procedure is available via the repository Chemotion: https://dx.doi.org/10.14272/reaction/SA-FUHFF-UHFFFADPSC-ZVVVMNPCOQ-UHFFFADPSC-NUHFF-MUHFF-NUHFF-ZZZ (accessed on 22 July 2024).

Additional information on the characterization of the target compound is available via the repository Chemotion: https://dx.doi.org/10.14272/ZVVVMNPCOQCMKO-UHFFFAOYSA-M.1 (accessed on 22 July 2024).

3.3. Synthesis of the Binuclear Cu(I) Complexes

Copper(I) chloride (50.0 mg, 505 µmol, 1.00 equiv) was dissolved in 10 mL of dry DCM together with triphenylphosphine (265 mg, 1.01 mmol, 2.00 equiv) or DPEPhos (272 mg, 505 µmol, 1.00 equiv) under an Ar atmosphere. After stirring for 1 h, 2,1,3-benzoselenadiazole (92.5 mg, 505 µmol, 1.00 equiv) and silver(I) perchlorate (105 mg, 505 µmol, 1.00 equiv) were added to the reaction media, and the color of the solution rapidly changed to red. The mixture was stirred for 18 h at 20 °C, and the precipitated AgCl was filtered off to afford a clear solution that was evaporated under reduced pressure. The so-obtained oil was treated with diethyl ether to afford a solid that was filtered off, washed with Et_2O (2 × 5 mL), and dried in vacuo. The products, $[Cu_2(\mu_2\text{-BSeD})(PPh_3)_4][ClO_4]_2$ and $[Cu_2(BSeD)(\mu_2\text{-DPEphos})_2][ClO_4]_2$, were respectively isolated as an orange (369 mg, 225 µmol, 89% yield) and a dark red solid (353 mg, 223 µmol, 84% yield).

Characterization of $[Cu_2(\mu_2\text{-BSeD})(PPh_3)_4(ClO_4)_2]$. m.p.: 170 °C (dec.). ^{1}H NMR (400 MHz, Chloroform-d [7.27 ppm], ppm) δ = 7.62 (t, *J* = 7.9 Hz, 1H, BSeD), 7.55–7.45 (m, 3H, BSeD), 7.42–7.30 (m, 36H, PPh_3), 7.28–7.25 (m, 24H, PPh_3). ^{31}P{^{1}H} NMR (162 MHz, ppm) δ = −0.37 (br.s). ^{13}C NMR (100 MHz, Chloroform-d [77.0 ppm], ppm) δ = 159.2 (Cq,

2C), 133.9 (d, *J* = 8.4 Hz, 24C), 131.0 (d, *J* = 32.7 Hz, Cq, 12C), 130.6 (CH, 12C), 130.1 (CH, 2C), 129.1 (CH, 24C), 123.2 (CH, 2C). MS (ESI), *m*/*z* (%): 852 (7), 851 (12) $[Cu(PPh_3)_3]^+$, 850 (18), 849 (31), 633 (12), 632 (5), 631 (13), 605 (7), 604 (6), 603 (16), 590 (16), 589 (42), 588 (39), 587 (100) $[Cu(PPh_3)_2]^+$. IR (ATR, $\tilde{\nu}$) = 3072 (vw), 3055 (vw), 1479 (w), 1435 (m), 1160 (vw), 1147 (w), 1113 (m), 1094 (vs), 1035 (s), 1027 (s), 996 (m), 973 (w), 924 (w), 902 (w), 742 (vs), 727 (w), 693 (vs), 618 (m), 517 (vs), 500 (vs), 442 (w), 429 (w), 391 (w) cm^{-1}. EA ($C_{78}H_{64}Cl_2Cu_2N_2O_8P_4Se$): Calcd C, 60.12; H, 4.14; N, 1.80. Found C, 59.19; H, 3.88; N, 1.90.

Additional information on the experimental procedure is available via the repository Chemotion: https://dx.doi.org/10.14272/reaction/SA-FUHFF-UHFFFADPSC-IJTSCRZYFP-UHFFFADPSC-NUHFF-LUHFF-NUHFF-ZZZ (accessed on 22 July 2024).

Additional information on the characterization of the target compound is available via the repository Chemotion: https://dx.doi.org/10.14272/IJTSCRZYFPRHQA-UHFFFAOYSA-L.1 (accessed on 22 July 2024).

Characterization of $[Cu_2(\mu_2\text{-BSeD})(DPEphos)_2(ClO_4)_2]$. m.p.: 226 °C (dec.). ^1H NMR (400 MHz, Chloroform-d [7.27 ppm], ppm) δ = 7.52–7.50 (m, 2H, BSeD), 7.26–7.06 (m, 48H, BSeD + DPEphos), 6.91 (t, *J* = 7.5 Hz, 6H, DPEphos), 6.69 (dt, *J* = 3.9 Hz, *J* = 8.0 Hz, 4H, DPEphos). $^{31}P\{^1H\}$ NMR (162 MHz, ppm) δ = −15.93 (br.s). ^{13}C NMR (100 MHz, Chloroform-d [77.0 ppm], ppm) δ = 158.9 (Cq, 2C), 134.4 (t, *J* = 5.9 Hz, Cq, 4C), 134.0 (CH, 4C), 133.9 (t, *J* = 8.0 Hz, CH, 16C), 131.9 (CH, 6C), 130.4 (CH, 8C), 130.0 (t, *J* = 17.8 Hz, Cq, 8C), 129.8 (CH, 2C), 128.9 (t, *J* = 4.5 Hz, CH, 16C), 125.0 (CH, 6C), 123.9 (t, *J* = 15.4 Hz, Cq, 2C), 122.9 (CH, 2C), 119.8 (Cq, 2C). MS (ESI), *m*/*z* (%): 1242 (5), 1241 (6), 1240 (14), 1239 (19), 1238 (12), 1237 (15), 604 (16), 603 (44), 602 (40), 601 (100) $[Cu(DPEphos)]^+$. IR (ATR, $\tilde{\nu}$) = 3064 (vw), 3051 (vw), 1480 (w), 1462 (w), 1434 (vs), 1259 (w), 1204 (s), 1162 (w), 1119 (s), 1094 (s), 1068 (s), 1026 (vs), 999 (m), 907 (w), 897 (w), 871 (w), 866 (w), 802 (w), 765 (w), 742 (vs), 694 (vs), 671 (w), 616 (s), 543 (w), 530 (w), 520 (m), 511 (vs), 500 (s), 494 (s), 480 (s), 465 (m), 450 (w), 429 (w), 414 (w), 390 (w) cm^{-1}. EA ($C_{78}H_{60}Cl_2Cu_2N_2O_{10}P_4Se$): Calcd C, 67.53; H, 4.36; N, 2.02. Found C, 58.49; H, 3.63; N, 2.33.

Additional information on the experimental procedure is available via the repository Chemotion: https://dx.doi.org/10.14272/reaction/SA-FUHFF-UHFFFADPSC-MGDYVPDVFV-UHFFFADPSC-NUHFF-LUHFF-NUHFF-ZZZ (accessed on 22 July 2024).

Additional information on the characterization of the target compound is available via the repository Chemotion: https://dx.doi.org/10.14272/MGDYVPDVFVURBP-UHFFFAOYSA-L.1 (accessed on 22 July 2024).

3.4. Crystal Structure Determination

Single crystal X-ray diffraction data were collected on a STOE (Darmstadt, Germany) STADIVARI diffractometer with monochromated Mo-Kα (λ = 0.71073 Å) radiation at 180 K. Using Olex2 version 1.5 [37], the structures were solved with the SHELXT version 2019 [38] structure solution program using intrinsic phasing and refined with the SHELXL version 2019 [39] refinement package using least-squares minimization. Refinement was performed with anisotropic temperature factors for all non-hydrogen atoms; hydrogen atoms were calculated on idealized positions. Details regarding the crystal data and structural refinement are given in Table 1. Selected bond lengths and angles are collected in Tables S1 and S2.

Deposition Numbers CCDC-2353339 and CCDC-2353340 contain the supplementary crystallographic data for this paper. These data are provided free of charge by the joint Cambridge Crystallographic Data Centre and Fachinformationszentrum Karlsruhe https://www.ccdc.cam.ac.uk/structures/ (accessed on 22 July 2024) Access Structures service.

3.5. Photoluminescent Measurements

The absorption spectra were collected in dichloromethane solutions employing an Analytik Jena Specord 50 instrument (Jena, Germany). Room temperature photoluminescence emission (PL) and excitation (PLE) spectra were collected on powder samples using a Horiba (Kyoto, Japan) Fluorolog-3C-22 spectrofluorometer equipped with a 450 W Xenon

lamp. Suitable long-pass filters were placed in front of the acquisition systems to avoid second-order effects. Photoluminescent lifetimes τ were recorded employing multi-channel scaling modality (MCS) triggering the Xe lamp. Photoluminescence quantum yield Φ was measured on solid samples using a Horiba (Kyoto, Japan) Quanta Phi integrating sphere.

3.6. DFT Calculations

The ground-state geometries optimization was carried out using the range-separate hybrid DFT functional TPSSh in combination with Ahlrichs and Weigend's def2 split-valence polarized (def2-SVP) basis set [40–42]. IR simulations were carried out to confirm reaching a minimum in the calculations. The C-PCM implicit solvation model was added to the calculations, considering dichloromethane as a continuous medium [43,44], as well as the D4 model for the dispersion interaction [45]. Excited states and their relative energies were investigated employing TDDFT (time-dependent DFT) calculations at the same theoretical level [46]. This method was chosen to investigate the photophysical properties, including the spin-orbit coupling, in the computations [47]. The calculations were carried out with ORCA 5.0.4 through the bwHPC cluster [48,49], and the output files were analysed with Multiwfn, version 3.8 [50,51]. Cartesian coordinates of the DFT-optimized structures are provided in Table S8.

4. Conclusions

In this study, 2,1,3-benzoselenadiazole (BSeD) was successfully employed as a mono- and bidentate N-donor ligand for the preparation of heteroleptic Cu(I) complexes with triphenylphosphine and bis[(2-diphenylphosphino)phenyl] ether (DPEphos) in the coordination sphere. The species were isolated via displacement reaction on Cu(I) chloride in the presence of $AgClO_4$. The proposed formulae were supported by common spectroscopic techniques together with ^{77}Se NMR, which was recorded both for the free ligand and the three derived Cu(I) complexes. In some cases, the structure was further elucidated by single-crystal X-ray diffraction. All the derivatives were intensely colored as powder and in concentrated solutions, with intense absorptions below 400 nm. The Cu(I) species with the general formula $[Cu(BSeD)(PPh_3)_2(ClO_4)]$ and $[Cu_2(\mu_2\text{-}BSeD)(PPh_3)_4(ClO_4)_2]$ were characterized by weak emissions around 700 nm with lifetimes τ in the μs range, suggesting the involvement of triplet emitting states. This outcome was supported by TDDFT calculations, which were carried out on the optimized ground state geometries and with the introduction of the spin-orbit coupling in the computations. To conclude, the introduction of a heavier chalcogen atom, i.e., selenium, in the skeleton of the N-donor was found to have a deleterious effect on the intensity and the lifetime of the emission compared to the previously reported BTD Cu(I) derivatives, due to the increased spin-orbit coupling effect and consequently the higher rate of the intersystem crossing.

Supplementary Materials: The following supporting information can be downloaded at: https://www.mdpi.com/article/10.3390/inorganics12080201/s1, Table S1: Selected bond lengths [Å] and angles [°] for $[Cu(BSeD)(PPh_3)_2(ClO_4)]$; Table S2: Selected bond lengths [Å] and angles [°] for $[Cu_2(\mu_2\text{-}BSeD)(DPEphos)_2(ClO_4)_2]$; Table S3: Hydrogen bonds parameters for $[Cu(BSeD)(PPh_3)_2(ClO_4)]$; Table S4: Hydrogen bonds parameters for $[Cu_2(\mu_2\text{-}BSeD)(DPEphos)_2(ClO_4)_2]$; Figure S1: Pictures of the complexes as powder and in 0.02 M DCM solution; Figure S2: UV-vis spectra of the complexes in the range 330–550 nm; Table S5: Selected bond lengths [Å] and angles [°] for $[Cu(BSeD)(PPh_3)_2(ClO_4)]$ obtained through DFT calculations; Figure S3: Overlapping the structures of $[Cu(BSeD)(PPh_3)_2(ClO_4)]$ obtained through X-ray diffraction and DFT calculations; Table S6: Selected bond lengths [Å] and angles [°] for $[Cu_2(\mu_2\text{-}BSeD)(DPEphos)_2(ClO_4)_2]$ obtained through DFT calculations; Figure S4: Overlapping structures of $[Cu_2(\mu_2\text{-}BSeD)(DPEphos)_2(ClO_4)_2]$ obtained through X-ray diffraction and DFT calculations; Figure S5: DFT-optimized structure of $[Cu(BSeD)(PPh_3)_2(ClO_4)]$ and selected (3,−1) BPCs; Figure S6: DFT-optimized structure of $[Cu_2(\mu_2\text{-}BSeD)(DPEphos)_2(ClO_4)_2]$ and selected (3,−1) BPCs. Figure S7: HOMO and LUMO plot of $[Cu(BSeD)(PPh_3)_2(ClO_4)]$ obtained through TDDFT calculations; Table S8: Cartesian coordinates of the DFT-optimized ground singlet state structures of $[Cu(BSeD)(PPh_3)_2(ClO_4)]$ and $[Cu_2(\mu_2\text{-}BSeD)(DPEphos)_2(ClO_4)_2]$.

Author Contributions: Conceptualization, V.F. and S.B.; methodology, V.F., F.H., O.F., B.L. and S.B.; validation, V.F., F.H., B.L. and S.B.; formal analysis, V.F., F.H. and O.F.; investigation, V.F., F.H. and O.F.; resources, V.F., F.H., O.F., B.L. and S.B.; data curation, V.F., F.H., O.F., B.L. and S.B.; writing—original draft preparation, V.F., F.H., O.F., B.L. and S.B.; writing—review and editing, V.F., F.H., O.F., B.L. and S.B.; visualization, V.F., F.H., O.F., B.L. and S.B.; supervision, B.L. and S.B.; project administration, B.L. and S.B.; funding acquisition, B.L. and S.B. All authors have read and agreed to the published version of the manuscript.

Funding: This research was funded by the Deutsche Forschungsgemeinschaft (DFG, German Research Foundation) under Germany's Excellence Strategy via the Excellence Cluster "3D Matter Made to Order" (3DMM2O, EXC-2082/1–390761711).

Data Availability Statement: The details on the chemical synthesis and original analytical data were added to the repository Chemotion (www.chemotion.net/home, accessed on 22 July 2024) [35].

Acknowledgments: The authors acknowledge support by the state of Baden-Württemberg through bwHPC, the German Research Foundation (DFG) through grant no INST 40/575-1 FUGG (JUSTUS 2 cluster), and IFG (KIT) for the access to the Horiba instrument. V.F. sincerely thanks Jésus Castro (University of Vigo) for the fruitful discussions concerning the X-ray structures.

Conflicts of Interest: The authors declare no conflicts of interest.

References

1. Findlay, N.J.; Breig, B.; Forbes, C.; Inigo, A.R.; Kanibolotsky, A.L.; Skabara, P.J. High brightness solution-processed OLEDs employing linear, small molecule emitters. *J. Mater. Chem. C* **2016**, *4*, 3774–3780. [CrossRef]
2. Wu, Y.; Zhu, W. Organic sensitizers from D–π–A to D–A–π–A: Effect of the internal electron-withdrawing units on molecular absorption, energy levels and photovoltaic performances. *Chem. Soc. Rev.* **2013**, *42*, 2039–2058. [CrossRef] [PubMed]
3. Neto, B.A.D.; Lapis, A.A.M.; Da Silva Júnior, E.N.; Dupont, J. 2,1,3-Benzothiadiazole and Derivatives: Synthesis, Properties, Reactions, and Applications in Light Technology of Small Molecules. *Eur. J. Org. Chem.* **2013**, *2013*, 228–255. [CrossRef]
4. Du, J.; Biewer, M.C.; Stefan, M.C. Benzothiadiazole building units in solution-processable small molecules for organic photovoltaics. *J. Mater. Chem. A* **2016**, *4*, 15771–15787. [CrossRef]
5. Neto, B.A.; Carvalho, P.H.; Correa, J.R. Benzothiadiazole Derivatives as Fluorescence Imaging Probes: Beyond Classical Scaffolds. *Acc. Chem. Res.* **2015**, *48*, 1560–1569. [CrossRef]
6. Li, C.C.; Cao, J.; Wang, L.; Ji, X.; Xu, Y.; Wang, J.Y. π-Extended BTD Derivatives: Synthesis, Photophysical Properties, and Applications in Biological Systems Imaging for Discriminating Living and Dead Cells. *Chem. Asian J.* **2023**, *18*, e202300038. [CrossRef]
7. Chen, C.-P.; Wu, P.-J.; Liou, S.-Y.; Chan, Y.-H. Ultrabright benzoselenadiazole-based semiconducting polymer dots for specific cellular imaging. *RSC Adv.* **2013**, *3*, 17507. [CrossRef]
8. Patel, H.A.; Bhanvadia, V.J.; Mande, H.M.; Zade, S.S.; Patel, A.L. Benzochalcogendiazole-based conjugated molecules: Investigating the effects of substituents and heteroatom juggling. *Org. Biomol. Chem.* **2019**, *17*, 9467–9478. [CrossRef]
9. Li, H.; Chi, Z.; Zhang, X.; Xu, B.; Liu, S.; Zhang, Y.; Xu, J. New thermally stable aggregation-induced emission enhancement compounds for non-doped red organic light-emitting diodes. *Chem. Commun.* **2011**, *47*, 11273. [CrossRef]
10. Gao, S.; Balan, B.; Yoosaf, K.; Monti, F.; Bandini, E.; Barbieri, A.; Armaroli, N. Highly Efficient Luminescent Solar Concentrators Based on Benzoheterodiazole Dyes with Large Stokes Shifts. *Chem. Eur. J.* **2020**, *26*, 11013–11023. [CrossRef]
11. Ho, P.C.; Wang, J.Z.; Meloni, F.; Vargas-Baca, I. Chalcogen bonding in materials chemistry. *Coord. Chem. Rev.* **2020**, *422*, 213464. [CrossRef]
12. Bryant, J.J.; Lindner, B.D.; Bunz, U.H. Water-soluble bis-triazolyl benzochalcogendiazole cycloadducts as tunable metal ion sensors. *J. Org. Chem.* **2013**, *78*, 1038–1044. [CrossRef] [PubMed]
13. Ferraro, V.; Girotto, M.; Castro, J.; Bortoluzzi, M. Intense millisecond-long red luminescence from heteroleptic Cu(I) 2,1,3-benzothiadiazole complexes. *Dye. Pigm.* **2023**, *217*, 111388. [CrossRef]
14. Busch, J.M.; Rehak, F.R.; Ferraro, V.; Nieger, M.; Kemell, M.; Fuhr, O.; Klopper, W.; Bräse, S. From Mono- to Polynuclear 2-(Diphenylphosphino)pyridine-Based Cu(I) and Ag(I) Complexes: Synthesis, Structural Characterization, and DFT Calculations. *ACS Omega* **2024**, *9*, 2220–2233. [CrossRef] [PubMed]
15. Ferraro, V.; Fuhr, O.; Bizzarri, C.; Bräse, S. Substituted Pyrrole-based Schiff Bases: Effect on The Luminescence of Neutral Heteroleptic Cu(I) Complexes. *Eur. J. Inorg. Chem.* **2024**, *27*, e202400080. [CrossRef]
16. Fang, Y.; Zhu, K.; Teat, S.J.; Reid, O.G.; Hei, X.; Zhu, K.; Fang, X.; Li, M.; Sojdak, C.A.; Cotlet, M.; et al. Robust and Highly Conductive Water-Stable Copper Iodide-Based Hybrid Single Crystals. *Chem. Mater.* **2022**, *34*, 10040–10049. [CrossRef]
17. Sukhikh, T.S.; Khisamov, R.M.; Bashirov, D.A.; Komarov, V.Y.; Molokeev, M.S.; Ryadun, A.A.; Benassi, E.; Konchenko, S.N. Tuning of the Coordination and Emission Properties of 4-Amino-2,1,3-Benzothiadiazole by Introduction of Diphenylphosphine Group. *Cryst. Growth Des.* **2020**, *20*, 5796–5807. [CrossRef]

18. Plebst, S.; Bubrin, M.; Schweinfurth, D.; Záliš, S.; Kaim, W. Metal carbonyl complexes of potentially ambidentate 2,1,3-benzothiadiazole and 2,1,3-benzoselenadiazole acceptors. *Z. Naturforsch. B* **2017**, *72*, 839–846. [CrossRef]
19. Herberhold, M.; Hill, A.F. The coordination chemistry of 2,1,3-benzothiadiazole and 2,1,3-benzoselenadiazole. Complexes of ruthenium, osmium and iridium. *J. Organomet. Chem.* **1989**, *377*, 151–156. [CrossRef]
20. Cowley, A.R.; Hector, A.L.; Hill, A.F.; White, A.J.P.; Williams, D.J.; Wilton-Ely, J.D.E.T. Synthesis and Reactions of Five-Coordinate Mono- and Binuclear Thiocarbonyl−Alkenyl and Thioacyl Complexes of Ruthenium (II). *Organometallics* **2007**, *26*, 6114–6125. [CrossRef]
21. Tan, C.K.; Wang, J.; Leng, J.D.; Zheng, L.L.; Tong, M.L. The Use of 2,1,3-Benzoselenadiazole as an Auxiliary Ligand for the Construction of New 2D Silver(I)/Benzene- or Cyclohexane-1,3,5-tricarboxylate Honeycomb Networks. *Eur. J. Inorg. Chem.* **2008**, *2008*, 771–778. [CrossRef]
22. Milios, C.J.; Ioannou, P.V.; Raptopoulou, C.P.; Papaefstathiou, G.S. Crystal engineering with 2,1,3-benzoselenadiazole and mercury (II) chloride. *Polyhedron* **2009**, *28*, 3199–3202. [CrossRef]
23. Mitra, R.; Sridevi, V.S.; Somasundaram, K.; Samuelson, A.G. Photophysical and Biological Studies with Organometallic Ruthenium Complexes of Selenodiazole Ligands. *Proc. Natl. Acad. Sci. India A* **2016**, *86*, 511–520. [CrossRef]
24. Sysoeva, A.A.; Novikov, A.S.; Suslonov, V.V.; Bolotin, D.S.; Il'in, M.V. 2,1,3-Benzoselenadiazole-containing zinc (II) halide complexes: Chalcogen bonding in the solid state and catalytic activity in the Schiff condensation. *Inorg. Chim. Acta* **2024**, *561*, 121867. [CrossRef]
25. Parsons, S. Determination of absolute configuration using X-ray diffraction. *Tetrahedron: Asymmetry* **2017**, *28*, 1304–1313. [CrossRef]
26. Cordero, B.; Gómez, V.; Platero-Prats, A.E.; Revés, M.; Echeverría, J.; Cremades, E.; Barragán, F.; Alvarez, S. Covalent radii revisited. *Dalton Trans.* **2008**, *21*, 2832. [CrossRef] [PubMed]
27. Bera, J.K.; Nethaji, M.; Samuelson, A.G. Synthesis and Structures of Oxyanion Encapsulated Copper(I)−dppm Complexes (dppm = Bis(diphenylphosphino)methane). *Inorg. Chem.* **1999**, *38*, 1725. [CrossRef] [PubMed]
28. Mao, S.; Han, X.; Li, C.; Xu, Y.; Shen, K.; Shi, X.; Wu, H. Cu(I) complexes regulated by N-heterocyclic ligands: Syntheses, structures, fluorescence and electrochemical properties. *Spectrochim. Acta A* **2018**, *203*, 408. [CrossRef]
29. Chou, C.-C.; Su, C.-C.; Yeh, A. Mononuclear and Dinuclear Copper(I) Complexes of Bis(3,5-dimethylpyrazol-1-yl) methane: Synthesis, Structure, and Reactivity. *Inorg. Chem.* **2005**, *44*, 6122–6128. [CrossRef]
30. Fujisawa, K.; Noguchi, Y.; Miyashita, Y.; Okamoto, K.; Lehnert, N. Mononuclear and Binuclear Copper(I) Complexes Ligated by Bis(3,5-diisopropyl-1-pyrazolyl) methane: Insight into the Fundamental Coordination Chemistry of Three-Coordinate Copper(I) Complexes with a Neutral Coligand. *Inorg. Chem.* **2007**, *46*, 10607–10623. [CrossRef]
31. Bianchi, R.; Gervasio, G.; Marabello, D. Experimental Electron Density Analysis of $Mn_2(CO)_{10}$: Metal-Metal and Metal-Ligand Bond Characterization. *Inorg. Chem.* **2000**, *39*, 2360–2366. [CrossRef] [PubMed]
32. Lepetit, C.; Fau, P.; Fajerwerg, K.; Kahn, M.L.; Silvi, B. Topological analysis of the metal-metal bond: A tutorial review. *Coord. Chem. Rev.* **2017**, *345*, 150–181. [CrossRef]
33. Yang, X.; Chin, R.M.; Hall, M.B. Protonating metal-metal bonds: Changing the metal-metal interaction from bonding, to nonbonding, and to antibonding. *Polyhedron* **2022**, *212*, 115585. [CrossRef]
34. Beaudelot, J.; Oger, S.; Perusko, S.; Phan, T.A.; Teunens, T.; Moucheron, C.; Evano, G. Photoactive Copper Complexes: Properties and Applications. *Chem. Rev.* **2022**, *122*, 16365–16609. [CrossRef] [PubMed]
35. Ferraro, V.; Bräse, S. Chemotion Repository. Available online: https://doi.org/10.14272/collection/VF_2024-03-05 (accessed on 22 July 2024).
36. Enders, M.; Görling, B.; Braun, A.B.; Seltenreich, J.E.; Reichenbach, L.F.; Rissanen, K.; Nieger, M.; Luy, B.; Schepers, U.; Bräse, S. Cytotoxicity and NMR Studies of Platinum Complexes with Cyclooctadiene Ligands. *Organometallics* **2014**, *33*, 4027–4034. [CrossRef]
37. Dolomanov, O.V.; Bourhis, L.J.; Gildea, R.J.; Howard, J.A.K.; Puschmann, H. *OLEX2*: A complete structure solution, refinement and analysis program. *J. Appl. Crystallogr.* **2009**, *42*, 339–341. [CrossRef]
38. Sheldrick, G.M. SHELXT—Integrated space-group and crystal-structure determination. *Acta Crystallogr. A Found. Adv.* **2015**, *71*, 3–8. [CrossRef] [PubMed]
39. Sheldrick, G.M. Crystal structure refinement with SHELXL. *Acta Crystallogr. Sect. C Struct. Chem.* **2015**, *71*, 3–8. [CrossRef] [PubMed]
40. Staroverov, V.N.; Scuseria, G.E.; Tao, J.; Perdew, J.P. Comparative assessment of a new nonempirical density functional: Molecules and hydrogen-bonded complexes. *J. Chem. Phys.* **2003**, *119*, 12129–12137. [CrossRef]
41. Bühl, M.; Kabrede, H. Geometries of Transition-Metal Complexes from Density-Functional Theory. *J. Chem. Theory Comput.* **2006**, *2*, 1282–1290. [CrossRef]
42. Weigend, F.; Ahlrichs, R. Balanced basis sets of split valence, triple zeta valence and quadruple zeta valence quality for H to Rn: Design and assessment of accuracy. *Phys. Chem. Chem. Phys.* **2005**, *7*, 3297. [CrossRef] [PubMed]
43. Barone, V.; Cossi, M. Quantum Calculation of Molecular Energies and Energy Gradients in Solution by a Conductor Solvent Model. *J. Phys. Chem. A* **1998**, *102*, 1995–2001. [CrossRef]
44. Cossi, M.; Rega, N.; Scalmani, G.; Barone, V. Energies, structures, and electronic properties of molecules in solution with the C-PCM solvation model. *J. Comput. Chem.* **2003**, *24*, 669–681. [CrossRef] [PubMed]

45. Spicher, S.; Caldeweyher, E.; Hansen, A.; Grimme, S. Benchmarking London dispersion corrected density functional theory for noncovalent ion–π interactions. *Phys. Chem. Chem. Phys.* **2021**, *23*, 11635–11648. [CrossRef] [PubMed]
46. Ullrich, C.A. *Time-Dependent Density Functional Theory*; Oxford University Press: Oxford, UK, 2012.
47. De Souza, B.; Farias, G.; Neese, F.; Izsák, R. Predicting Phosphorescence Rates of Light Organic Molecules Using Time-Dependent Density Functional Theory and the Path Integral Approach to Dynamics. *J. Chem. Theory Comput.* **2019**, *15*, 1896–1904. [CrossRef] [PubMed]
48. Neese, F.; Wennmohs, F.; Becker, U.; Riplinger, C. The ORCA quantum chemistry program package. *J. Chem. Phys.* **2020**, *152*, 224108. [CrossRef] [PubMed]
49. Neese, F. Software update: The ORCA program system—Version 5.0. *WIREs Comput. Mol. Sci.* **2022**, *12*, e1606. [CrossRef]
50. Lu, T.; Chen, F. Multiwfn: A multifunctional wavefunction analyzer. *J. Comput. Chem.* **2012**, *33*, 580–592. [CrossRef]
51. Liu, Z.; Lu, T.; Chen, Q. An sp-hybridized all-carboatomic ring, cyclo [18] carbon: Electronic structure, electronic spectrum, and optical nonlinearity. *Carbon* **2020**, *165*, 461–467. [CrossRef]